Article

Employing Molecular Docking Calculations for the Design of Alkyl (2-Alcoxy-2-Hydroxypropanoyl)-*L*-Tryptophanate Derivatives as Potential Inhibitors of 11β-Hydroxysteroid Dehydrogenase Type 1 (11β-HSD1)

Diego Quiroga (ID)

Bioorganic Chemistry Laboratory, Facultad de Ciencias Básicas y Aplicadas, Universidad Militar Nueva Granada, Campus Nueva Granada, Cajicá 250247, Colombia; diego.quiroga@unimilitar.edu.co

Abstract: In this paper, we presented the design by computational tools of novel alkyl (2-alcoxy-2-hydroxypropanoyl)-*L*-tryptophanate derivatives, which can be potential inhibitors of 11β-hydroxysteroid dehydrogenase type 1 (11β-HSD1). The molecular structure optimization of a group of 36 compounds was performed employing DFT-B3LYP calculations at the level 6-311G(d,p). Then, molecular docking calculations were performed using Autodock tools software, employing the Lamarckian genetic algorithm (LGA). Four parameters (binding, intermolecular and Van Der Waals hydrogen bonding desolvation energies, and HOMO-LUMO gap) were used to evaluate the potential as 11β-HSD1 inhibitors, which nominate *L*-tryptophan derivatives as the most promissory molecules. Finally, these molecules were obtained starting from the amino acid and pyruvic acid in a convergent methodology with moderate to low yields.

Keywords: 11β-hydroxysteroid dehydrogenase type 1; amino acids; *L*-tryptophan; hydroxypropanamide; amide

1. Introduction

11β-hydroxysteroid dehydrogenase type 1 (11β-HSD1) is a widely known enzyme, also known as cortisone reductase, which can be highly expressed in key metabolic tissues such as the liver, adipose tissue, and the central nervous system. Kotelevtsev [1] performed a targeted disruption of the 11β-HSD-1 gene in mice, demonstrating that these animals were unable to convert inert 11-dehydrocorticosterone to corticosterone in vivo. Those mice were found to resist hyperglycemia provoked by obesity or stress, evidencing the attenuation of hepatic 11β-HSD-1 provided a novel approach to the regulation of gluconeogenesis. Some studies [2–4] have suggested that 11β-HSD1 effectively amplifies the action of glucocorticoids in the liver, adipose tissue, and brain. Rask [3] evaluated the hypothalamic–pituitary–adrenal (HPA) axis and the activity of 11β-HSD1 in women with moderate obesity and insulin resistance, trying to find a relationship between Cushing's syndrome and metabolic syndrome, evidencing that in obese women a greater reactivation of glucocorticoids in fat contributes to the characteristics of metabolic syndrome. Tomlinson [4] discussed that the molecular basis of cortisone reductase deficiency, the putative "11β-HSD1 inactivation state" in humans, is caused by intronic mutations in HSD11B1 that decrease gene transcription together with mutations in hexose-6-phosphate dehydrogenase.

New protective effects of 11β-HSD1 deficiency on adipose function, distribution, and gene expression in vivo in nullizygous mice (11β-HSD1 −/−) of 11β-HSD-1 were reported [5], reporting the first in vivo evidence that adipose 11β-HSD-1 deficiency beneficially alters adipose tissue distribution and function, complementing the reported effects of liver 11β-HSD-1 deficiency or inhibition. Hermanowski-Vosatka [6] reported that the pharmacological inhibition of 11β-HSD1 has a therapeutic effect in mouse models of metabolic

syndrome. Its results showed that the administration of a selective and potent inhibitor of 11β-HSD1 reduced body weight, insulin, fasting glucose, triglycerides, and cholesterol in obese mice, and also slowed the progression of plaque in a murine model of atherosclerosis. Recently, some studies [6–11] probed other pathologies which involve 11β-HSD1, for example, depression and the risk of suicide. Studies with phenotypes allowed concluding that these polymorphs may be relevant biomarkers to detect genetically vulnerable subjects to a worse antidepressant response and a higher risk of suicide attempts [10]. These antecedents demonstrate that the inhibition of 11β-HSD1 represents a potential goal for the therapy of several disorders in humans.

The continuous research of novel bioactive molecules corresponds to one useful and versatile alternative to improve this goal. Wan [12] assessed piperazine sulfonamide derivatives, which showed high effectiveness and showed a significant reduction in fasting and food insulin and glucose levels when they were dosed orally in diet-induced obese mice. Structurally, this kind of molecule is of interest since it presents a hydroxypropanamide fragment and both sulfonamide and amide pharmacophores (Figure 1), to which several authors attributed its biological activity [13–21]. For example, Kamiński [14] synthesized some *N*-phenyl-2-(4-phenylpiperazin-1-yl)acetamide derivatives, which showed promising anticonvulsant activity in animal models of epilepsy. Tang [15] designed a series of new 2-hydroxyphenyl substituted aminoacetamides, which showed excellent antifungal activities against *S. sclerotiorum* and *P. capsici*. Shao [16] synthesized a new series of (sulfonamido)propanamides, which were evaluated against cell lines of hepatocellular carcinoma (HepG2), fibrosarcoma (HT-1080), epidermal carcinoma of the mouth (KB), and breast adenocarcinoma (MCF-7). Guo [17] developed a class of new dual-site tRNA-amino acid inhibitors versus threonyl-tRNA synthetase (ThrRS). Ibrahim [18] prepared unique flavopiridol analogs that contain thiosa sugars, amino acids, and heterocyclic residues anchored to flavopiridol through thioether and amine bonds mainly in its C ring, which demonstrated high cytotoxic activity in vitro against up to seven cancer cell lines. Zaręba [19] designed, synthesized, and evaluated new inhibitors of the uptake of γ-aminobutyric acid (GABA), membrane transport proteins that participate in the pathophysiology of several neurological disorders. Wasfy [20] synthesized phthalazine derivatives linked to amino acid derivatives with high yields. Phthalylamino acid derivatives showed potent antioxidant activity compared to standard drugs, and Wang [21] developed MET receptor kinase inhibitors of the type 5-((4-((2-amino-3-chloropyridin-4-yl)oxy)-3-fluorophenyl)amino)-3-(4-fluorophenyl)-1,6-naphthyridine-4(1*H*)-ones.
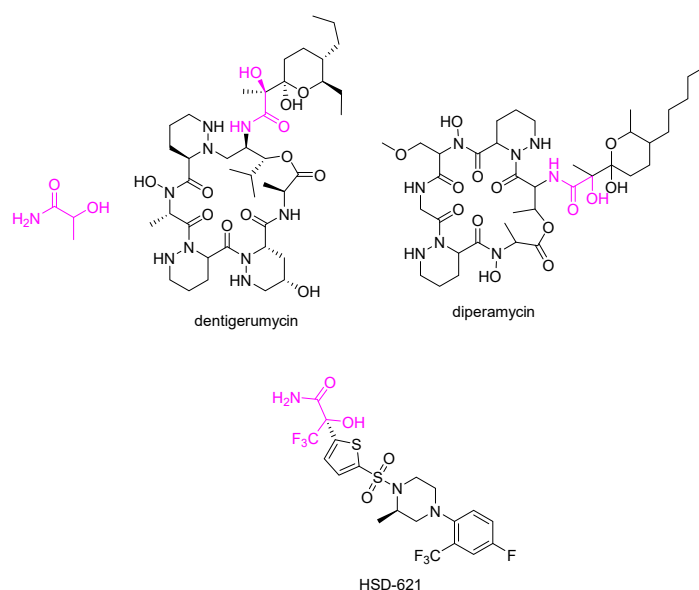

dentigerumycin

diperamycin

HSD-621

Figure 1. Hydroxypropanamide fragment, amide and sulfonamide pharmacophores in selected bioactive compounds.

Recently, Gregory [8] published a review discussing the use of 11β-HSD1 inhibitors in diseases associated with abnormalities in the function of the hypothalamic–pituitary–adrenal (HPA) axis. They identified around 1925 articles, proving to be a growing research field. Chuanxin [9] discussed the structural characteristics of the 11β-HSD1 inhibitors, the binding modes, the structure–activity relationships (SAR), and the biological evaluations of each inhibitor. These two reviews opened a paradigm regarding the development of new 11β-HSD1 inhibitors, especially regarding the need for rational design of new drugs based on computational strategies such as quantum mechanics calculations [22] and molecular docking [23] to predict the activity of new chemicals within its domain of applicability. Based on these tools, we performed the molecular design of 36 compounds with a hydroxypropanamide skeleton, which could be obtained from the conventional 2-aminoacids: *L*-tryptophane, *L*-alanine and *L*-phenylalanine, and pyruvic acid derivatives (Figure 2). These precursors were chosen knowing the multitarget use of pyruvic acid derivatives, such as DNA preservation by scavenging of the excess free radicals, antibiotic, anti-inflammatory, antioxidant, immunomodulatory, and anti-tumoral agents on many types of tumors, including pancreatic, prostate, liver, and gastric cancers [24–30]. The molecular docking results and the chemical synthesis of representative compounds are presented and discussed in this manuscript.
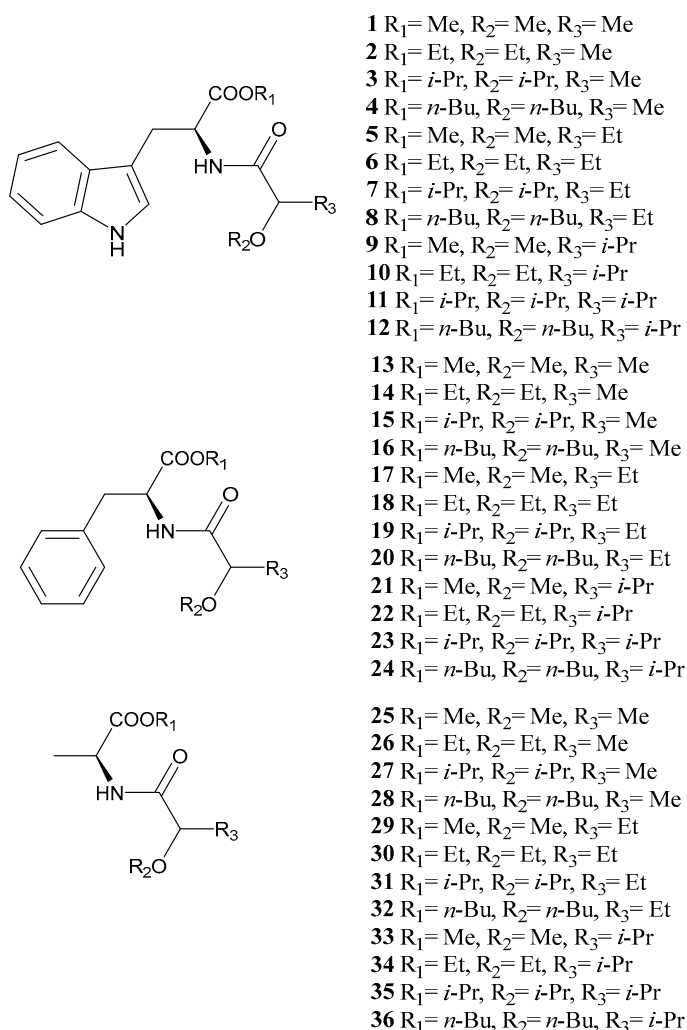

1 R_1= Me, R_2= Me, R_3= Me
2 R_1= Et, R_2= Et, R_3= Me
3 R_1= *i*-Pr, R_2= *i*-Pr, R_3= Me
4 R_1= *n*-Bu, R_2= *n*-Bu, R_3= Me
5 R_1= Me, R_2= Me, R_3= Et
6 R_1= Et, R_2= Et, R_3= Et
7 R_1= *i*-Pr, R_2= *i*-Pr, R_3= Et
8 R_1= *n*-Bu, R_2= *n*-Bu, R_3= Et
9 R_1= Me, R_2= Me, R_3= *i*-Pr
10 R_1= Et, R_2= Et, R_3= *i*-Pr
11 R_1= *i*-Pr, R_2= *i*-Pr, R_3= *i*-Pr
12 R_1= *n*-Bu, R_2= *n*-Bu, R_3= *i*-Pr

13 R_1= Me, R_2= Me, R_3= Me
14 R_1= Et, R_2= Et, R_3= Me
15 R_1= *i*-Pr, R_2= *i*-Pr, R_3= Me
16 R_1= *n*-Bu, R_2= *n*-Bu, R_3= Me
17 R_1= Me, R_2= Me, R_3= Et
18 R_1= Et, R_2= Et, R_3= Et
19 R_1= *i*-Pr, R_2= *i*-Pr, R_3= Et
20 R_1= *n*-Bu, R_2= *n*-Bu, R_3= Et
21 R_1= Me, R_2= Me, R_3= *i*-Pr
22 R_1= Et, R_2= Et, R_3= *i*-Pr
23 R_1= *i*-Pr, R_2= *i*-Pr, R_3= *i*-Pr
24 R_1= *n*-Bu, R_2= *n*-Bu, R_3= *i*-Pr

25 R_1= Me, R_2= Me, R_3= Me
26 R_1= Et, R_2= Et, R_3= Me
27 R_1= *i*-Pr, R_2= *i*-Pr, R_3= Me
28 R_1= *n*-Bu, R_2= *n*-Bu, R_3= Me
29 R_1= Me, R_2= Me, R_3= Et
30 R_1= Et, R_2= Et, R_3= Et
31 R_1= *i*-Pr, R_2= *i*-Pr, R_3= Et
32 R_1= *n*-Bu, R_2= *n*-Bu, R_3= Et
33 R_1= Me, R_2= Me, R_3= *i*-Pr
34 R_1= Et, R_2= Et, R_3= *i*-Pr
35 R_1= *i*-Pr, R_2= *i*-Pr, R_3= *i*-Pr
36 R_1= *n*-Bu, R_2= *n*-Bu, R_3= *i*-Pr

Figure 2. General molecular structure with substituents of the 36 molecules evaluated by quantum mechanics and molecular docking calculations.

2. Materials and Methods

2.1. General Information

All reagents and chemicals were commercially acquired (Merck KGaA (Darmstadt, Germany) and/or Sigma-Aldrich (St. Louis, MO, USA)) and were employed without additional refinement. The products' progression of reactions and purifications were monitored by thin-layer chromatography (TLC) on silica gel 60 F254 plates (Merck KGaA) under detection at 254 nm. Nuclear magnetic resonance (NMR) experiments were collected using a Bruker Avance AV-400 MHz spectrometer. TMS was used as a reference to give chemical shifts in δ (ppm). Typical splitting patterns were implemented to define the signal multiplicity (i.e., *s*, singlet; *d*, doublet; *t*, triplet; *m*, multiplet). Liquid chromatography-mass spectrometry (LC/MS) experiments were performed on an LCMS 2020 spectrometer (Shimadzu, Columbia, MD, USA), comprising a Prominence high-performance liquid chromatography (HPLC) system coupled to a single quadrupole analyzer with electrospray ionization (ESI). A Synergi column (150 × 4.6 mm, 4.0 µm) was used for analysis at 0.6 mL/min using mixtures of acetonitrile (A) and 1% formic acid (B) in gradient elution. The ESI was operated simultaneously in positive and negative ion modes (100–2000 m/z sweep), a desolvation line temperature of 250 °C, nitrogen as a nebulizer gas at 1.5 L/min, a drying at 8 L/min, and a detector voltage at 1.4 kV. High-resolution MS (HRMS) recorded accurate mass data on a microOTOF-Q II mass spectrometer (Bruker, Billerica, MA). The ESI was also operated in positive and negative ion modes (100–2000 m/z sweep), a desolvation line temperature of 250 °C, nitrogen as a nebulizer gas at 1.5 L/min, a drying at 8 L/min, quadrupole energy at 7.0 eV, and collision energy at 14 eV. The chemical reactions were carried out in a Discover System microwave reactor model 908005 series DY1030 in a closed vessel controlling the temperature.

2.2. Structural Optimization of the Proposed Compounds **1**–**36**

Optimization of all the compounds **1**–**36** was performed using the DFT-B3LYP method at the level 6-31G(d,p) [31,32]. Total energy and HOMO-LUMO gap were calculated and used as reactivity and stability descriptors. The crystal structure of 11β-HSD1 from an established structure (PDB ID: 1Y5M) file was downloaded from the protein data bank (www.rcsb.org accessed on 5 December 2022), previously reported by Zhang, obtaining the enzyme crystal using by the vapor diffusion method using hanging drops. The crystals structure belongs to space group P4122 with two molecules in the asymmetric unit. The ternary complex was obtained by soaking 0.05 mM corticosterone and 1 mM NADPH into the crystal [33].

2.3. Calculation of Molecular Docking and Bond-Free Energy

The boxes or grids were prepared using the Protein Grid Generation module, defining the box volume as 40 × 40 × 40 Å for all enzymes, to include all binding sites. Employing the active site of 11β-HSD1 reported by Thomas and Potter [34], the ligand–enzyme complexes were prepared and evaluated by molecular docking using the Lamarckian genetic algorithm (LGA) in the AutoDock v4.2.6 tools software [31].

2.4. Synthesis of Alkyl (2-Ethoxy-2-Hydroxypropanoyl)-L-Tryptophanate

A mixture of precursors 37 (1 eq) and 38 (1.1 eq) in the respective alcohol were heated at 150 °C for 15 min in the presence of triethylamine (TEA, 2 eq) in a microwave reactor in the open vessel mode. Then, the mixture was maintained overnight at room temperature until evaporation of the solvent. The product was purified using classic column chromatography using silica gel as sorbent for hexane: ethyl acetate mixtures as a mobile phase.

Methyl (2-methoxy-2-hydroxypropanoyl)-*L*-tryptophanate 1. Yield: 35%, yellow oil. ^{1}H NMR (400 MHz, CDCl₃) δ 8.20 (*s*, 1H), 7.52 (*s*, 1H), 7.39 (*d*, *J* = 8.2 Hz, 1H), 7.21 (*s*, 1H), 7.12 (*s*, 1H), 3.81 (*s*, 3H), 3.72 (*s*, 3H), 4.01–3.89 (*m*, 1H), 3.12 (*dd*, *J* = 15.2, 4.0 Hz, 1H), 2.83 (*dd*, *J* = 15.2, 4.0 Hz, 1H), 1.78 (*s*, 3H). ^{13}C NMR (101 MHz, CDCl₃) δ 172.0, 171.8, 136.8,

133.0, 126.8, 122.7, 119.9, 118.8, 111.4, 109.7, 62.2, 61.8, 59.2, 39.6, 35.3. ESI-MS in positive mode *m/z*: [M + H]⁺: 321.34.

Ethyl (2-ethoxy-2-hydroxypropanoyl)-*L*-tryptophanate 2. Yield: 57%, orange oil. ¹H NMR (400 MHz, CDCl₃) δ 8.19 (*s*, 1H), 7.51 (*s*, 1H), 7.38 (*d*, *J* = 8.2 Hz, 1H), 7.21 (*s*, 1H), 7.12 (*s*, 1H), 4.36–4.22 (*m*, 3H), 4.15 (*dq*, *J* = 10.8, 7.1 Hz, 1H), 3.95–3.86 (*m*, 1H), 3.14 (*dd*, *J* = 15.2, 4.0 Hz, 1H), 2.83 (*dd*, *J* = 15.2, 11.3 Hz, 1H), 1.75 (*s*, 3H), 1.63 (*s*, 1H), 1.36 (*t*, *J* = 7.1 Hz, 3H), 1.29 (*t*, *J* = 7.1 Hz, 3H). ¹³C NMR (101 MHz, CDCl₃) δ 174.0, 172.8, 136.8, 133.0, 126.8, 122.7, 120.0, 118.8, 111.4, 109.8, 62.7, 62.2, 61.6, 59.4, 54.4, 27.7, 25.6, 14.5. ESI-MS in positive mode *m/z*: [M + H]⁺: 349.15.

Methyl (3-methoxy-3-hydroxybutanoyl)-*L*-tryptophanate 5. Yield: 49%, yellow oil. ¹H NMR (400 MHz, CDCl₃) δ 8.21 (s, 1H), 7.49 (s, 1H), 7.37 (d, *J* = 8.2 Hz, 1H), 7.17 (s, 1H), 7.13 (*s*, 1H), 5.50 (*s*, 1H), 4.97 (*s*, 1H), 4.77–4.73 (*m*, 3H), 4.36–4.31 (*m*, 4H), 4.22 (*s*, 1H), 2.91 (*s*, 1H), 2.51 (*s*, 1H), 2.34 (*s*, 1H), 2.01–1.99 (*m*, 3H). ¹³C NMR (101 MHz, CDCl₃) δ 173.8, 172.9, 136.7, 133.0, 126.8, 122.7, 119.9, 118.8, 111.4, 109.8, 62.7, 62.2, 61.8, 59.4, 39.6, 37.38, 16.7. ESI-MS in positive mode *m/z*: [M + H]⁺: 335.37.

Ethyl (3-ethoxy-3-hydroxybutanoyl)-*L*-tryptophanate 6. Yield: 55%, yellow oil. ¹H NMR (400 MHz, CDCl₃) δ 8.20 (*s*, 1H), 7.50 (*s*, 1H), 7.40 (*d*, *J* = 8.2 Hz, 1H), 7.17 (*s*, 1H), 7.12 (*s*, 1H), 5.55 (*s*, 1H), 5.09 (*m*, 1H), 3.80–3.76 (*m*, 3H), 3.36–3.35 (*m*, 3H), 3.12 (*s*, 1H), 2.99 (*s*, 1H), 2.20 (*s*, 1H), 1.60–1.54 (*m*, 3H). ¹³C NMR (101 MHz, CDCl₃) δ 172.9, 171.6, 138.3, 128.0, 123.4, 121.7, 120.1, 119.5, 111.6, 108.5, 66.5, 61.8, 58.9, 52.5, 29.6, 28.2, 16.6, 14.7, 10.7. ESI-MS in positive mode *m/z*: [M + H]⁺: 363.42.

Propan-2-yl (2-oxopropanoyl)-*L*-tryptophanate 39. Yield: 71%, yellow oil. ¹H NMR (400 MHz, CDCl₃) δ 7.40 (*s*, 1H), 7.24–7.17 (*m*, 4H), 7.05 (*s*, 1H), 5.91 (*m*, 1H), 4.97 (*d*, *J* = 15.4 Hz, 2H), 3.32 (*s*, 1H), 2.88 (*s*, 1H), 2.31–2.27 (*m*, 3H), 1.43–1.31 (*m*, 6H). ¹³C NMR (101 MHz, CDCl₃) δ 193.1, 172.9, 163.6, 136.5, 128.3, 124.4, 121.7, 120.1, 119.5, 111.6, 108.5, 71.2, 52.8, 30.6, 25.1, 22.6. ESI-MS in positive mode *m/z*: [M + H]⁺: 349.15. HRMS in positive mode *m/z*: [M + H]⁺: experimental: 317.1496, calculated: 317.1503.

Propan-2-yl (3-oxobutanoyl)-*L*-tryptophanate 40. Yield: 65%, yellow oil. ¹H NMR (400 MHz, CDCl₃) δ 7.41 (*s*, 1H), 7.24–7.17 (*m*, 4H), 7.06 (*s*, 1H), 5.95 (*m*, 1H), 4.88 (*d*, *J* = 15.1 Hz, 2H), 3.31 (*s*, 1H), 3.11–2.97 (*m*, 2H), 2.89 (*s*, 1H), 1.43–1.31 (*m*, 6H), 1.19–1.15 (*m*, 3H). ¹³C NMR (101 MHz, CDCl₃) δ 193.8, 172.9, 160.8, 136.5, 128.3, 124.4, 121.7, 120.1, 119.6, 111.6, 108.5, 71.2, 52.8, 30.5, 26.4, 22.6, 10.6. ESI-MS in positive mode *m/z*: [M + H]⁺: 349.15. HRMS in positive mode *m/z*: [M + H]⁺: experimental: 331.1652, calculated: 331.1658.

3. Results and Discussion

The binding energy, intermolecular energy, and Van Der Waals hydrogen bonding desolvation energy were used as parameters for evaluation of the potential behavior of compounds **1**–**36** as 11β-HSD1 inhibitors. The results showed that the compounds derived from *L*-tryptophan have the lowest values for binding energy (−8.82 to −9.97 kcal/mol), suggesting that this amino acid could be considered the primary precursor of protein inhibitors (Table 1). This can be explained considering the presence of the indole group that facilitates the interaction with the active site, which is not present in the other molecules evaluated. Furthermore, regarding the HOMO-LUMO gap parameter, it can be seen that this class of molecules also presents the lowest values, indicating that they can be chemically active, facilitating both nucleophilic and electrophilic reactions in the active site of the enzyme. However, these values may also suggest lower stability of these derivatives than the compounds designed from the amino acids *L*-alanine and *L*-phenylalanine (**13**–**36**).

Table 1. Molecular docking and DFT-B3LYP calculated parameters for protein 11β-HSD1-ligands **1–36** complexes and single ligands.

Ligand	Binding Energy (kcal/mol)	Intermolecular Energy (kcal/mol)	Vdw Hb Desolvation Energy (kcal/mol)	HOMO-LUMO Gap (kcal/mol)
1	−8.82	−11.29	−11.11	4.87
2	−8.92	−11.93	−11.85	4.86
3	−8.83	−13.22	−13.15	4.89
4	−9.65	−12.94	−12.87	4.89
5	−8.87	−12.71	−12.63	4.88
6	−9.17	−13.29	−13.15	4.89
7	−9.04	−11.78	−11.58	4.89
8	−9.97	−13.49	−13.57	4.90
9	−9.52	−12.54	−12.37	4.88
10	−9.33	−13.63	−13.63	4.88
11	−9.92	−14.02	−13.93	4.88
12	−9.68	−12.71	−12.62	6.30
13	−8.65	−11.67	−11.65	6.26
14	−8.62	−11.92	−11.74	6.33
15	−7.72	−9.91	−9.83	6.48
16	−8.59	−12.98	−12.98	6.36
17	−8.16	−10.91	−10.82	6.22
18	−8.50	−11.25	−11.18	6.41
19	−7.84	−10.58	−10.50	6.39
20	−8.80	−12.10	−12.00	6.33
21	−8.38	−11.46	−11.38	6.22
22	−8.35	−10.82	−10.67	6.24
23	−7.83	−10.30	−10.24	6.26
24	−7.50	−11.07	−11.00	6.34
25	−7.46	−10.75	−10.60	6.05
26	−9.02	−12.04	−11.95	6.09
27	−7.33	−9.79	−9.61	6.13
28	−7.09	−9.56	−9.49	6.10
29	−6.93	−9.12	−9.15	6.01
30	−6.87	−10.44	−10.41	6.11
31	−6.72	−9.19	−9.03	6.12
32	−6.34	−8.54	−8.39	6.07
33	−6.23	−8.15	−8.03	6.00
34	−6.18	−8.65	−8.49	6.06
35	−6.09	−7.73	−7.64	6.07
36	−5.65	−7.57	−7.43	6.00

Molecular docking calculations allowed to obtain both ligand-target 2D and 3D diagrams (Figure 3), which showed the best fit for the molecule **8** and its interactions with different amino acid residues of the protein 11β-HSD1. The indolyl group of 8 approached a hydrophobic pocket surrounded by residual amino acids, Ile121, Ile46, and Asn119, although the latter was bonded through a conventional hydrogen bond. The alkyl hemiacetal fragment was surrounded by Tyr183, Leu126, and Ile227, forming the stable hydrophobic binding pattern. Moreover, a hydrogen bond interaction was established between the N-H amide group and the residual amino acid Tyr183. All these interactions supported compound 8 in the binding site of the 11β-HSD1.
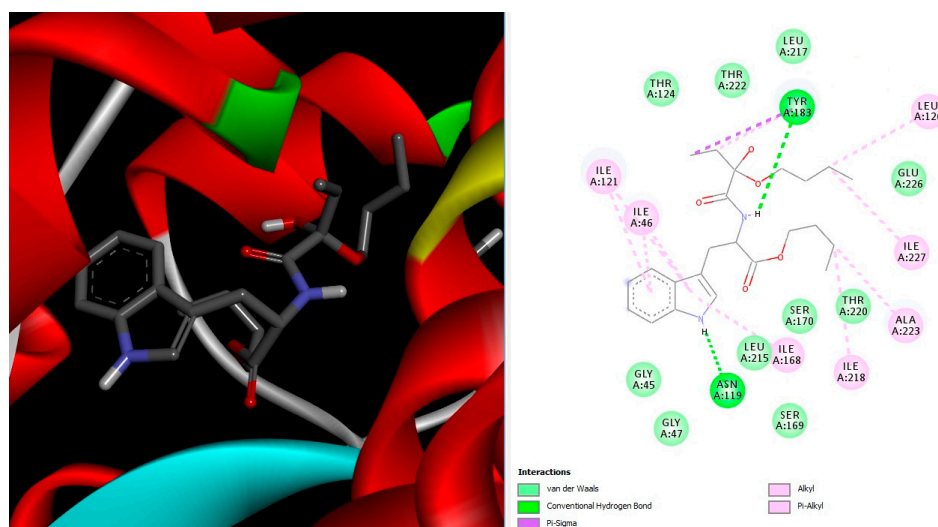
Figure 3. The 2D and 3D diagrams of the best-fit molecule **8** showing ligand interaction with different amino acid residues of the protein 11β-HSD1 in the active site.

Understanding that *L*-tryptophan derivatives **1–12** were the objective molecules according to the in silico results, we set out to establish a synthesis method for these molecules. The synthesis of these compounds usually employs a sequence of hydrolysis and Passerini reactions under ultrasound irradiation, using trifluoroacetophenones and isonitriles in acetic acid as starting reagents [35]. However, this synthetic method is not practical using 2-aminoacids as substrates. We performed an alternative synthesis method which is presented using this type of starting reagents. In this article, we presented the synthesis of **2** as model of the reaction, which was prepared by a convergent synthesis from precursor **37** and **38**. Precursor **37** was obtained via esterification of *L*-tryptophan [36] using $SiMe_3Cl$. Several preliminary amidation reaction experiments were carried out to obtain the optimized variables such as temperature, time, stoichiometric ratio, and influence of the substituents. The reaction between these precursors only occurs in basic medium, under temperatures close to 150 ° C under microwave irradiation (Scheme 1). The desired hydroxypropanamide compounds (**1–2**, **5–6**) were obtained using low molecular weight alcohols such as methanol and ethanol as the reaction medium. However, when the reaction was carried out in higher molecular weight alcohols, such as isopropanol, the major products were **39** and **40** with a moderate to high yield. In alcohols of higher molecular weight, no compounds other than the precursors were detected. These results suggest that the amidation reaction is kinetically favored under microwave irradiation conditions and that, subsequently, the presence of small alcohols (such as methanol and ethanol) leads to a subsequent reaction, in which the formation of a compound of the hemiacetal type takes place. When isopropanol is used, a transesterification and subsequent amidation initially occur, but the attack on the carbonyl group is not favored, so the hemiacetal described above is not formed.
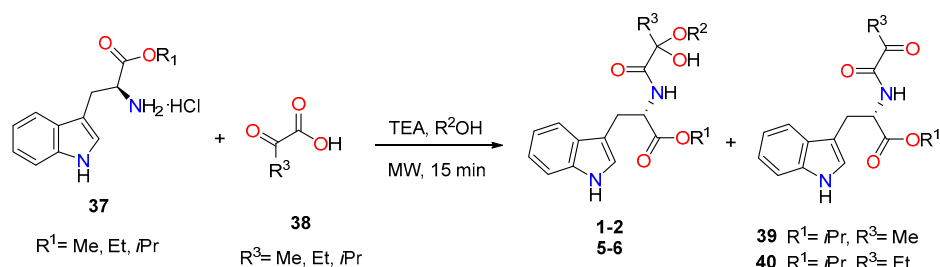
Scheme 1. Proposed synthetic method for amide derivatives of *L*-tryptophan.

4. Conclusions

In conclusion, based on computational calculations using quantum mechanics and molecular docking, we have designed, postulated, and synthesized (2-alcoxy-2-hydroxypropanoyl)-*L*-tryptophanate and alkyl (2-oxopropanoyl)-*L*-tryptophanate derivatives from *L*-tryptophan and pyruvic acid analogs, which can be considered as potential 11β-HSD1 inhibitors. The proposed synthetic method depends to a large extent on the precursor alcohol. In such a way, using low molecular weight alcohols, it was possible to obtain derivatives of the hemiacetal type, while high molecular weight alcohols favor the synthesis of the respective carbonyl compounds. In both cases, amidation is carried out, which is relevant since the presence of the amide group favors the potential behavior as an inhibitor of the protein.

References

1. Kotelevtsev, Y.; Holmes, M.C.; Burchell, A.; Houston, P.M.; Schmoll, D.; Jamieson, P.; Best, R.; Brown, R.; Edwards, C.R.W.; Seckl, J.R.; et al. 11β-Hydroxysteroid dehydrogenase type 1 knockout mice show attenuated glucocorticoid-inducible responses and resist hyperglycemia on obesity or stress. *Proc. Natl. Acad. Sci. USA* **1997**, *94*, 14924–14929. [CrossRef] [PubMed]
2. Seckl, J.R.; Walker, B.R. 11β-hydroxysteroid dehydrogenase type 1-A tissue-specific amplifier of glucocorticoid action. *Endocrinology* **2001**, *142*, 1371–1376. [CrossRef] [PubMed]
3. Rask, E.; Walker, B.R.; Söderberg, S.; Livingstone, D.E.W.; Eliasson, M.; Johnson, O.; Andrew, R.; Olsson, T. Tissue-specific changes in peripheral cortisol metabolism in obese women: Increased adipose 11β-hydroxysteroid dehydrogenase type 1 activity. *J. Clin. Endocrinol. Metab.* **2002**, *87*, 3330–3336. [CrossRef]
4. Tomlinson, J.W.; Walker, E.A.; Bujalska, I.J.; Draper, N.; Lavery, G.G.; Cooper, M.S.; Hewison, M.; Stewart, P.M. 11β-Hydroxysteroid dehydrogenase type 1: A tissue-specific regulator of glucocorticoid response. *Endocr. Rev.* **2004**, *25*, 831–866. [CrossRef]
5. Morton, N.M.; Paterson, J.M.; Masuzaki, H.; Holmes, M.C.; Staels, B.; Fievet, C.; Walker, B.R.; Flier, J.S.; Mullins, J.J.; Seckl, J.R. Novel Adipose Tissue-Mediated Resistance to Diet-Induced Visceral Obesity in 11β-Hydroxysteroid Dehydrogenase Type 1-Deficient Mice. *Diabetes* **2004**, *53*, 931–938. [CrossRef] [PubMed]
6. Hermanowski-Vosatka, A.; Balkovec, J.M.; Cheng, K.; Chen, H.Y.; Hernandez, M.; Koo, G.C.; Le Grand, C.B.; Li, Z.; Metzger, J.M.; Mundt, S.S.; et al. 11β-HSD1 inhibition ameliorates metabolic syndrome and prevents progression of atherosclerosis in mice. *J. Exp. Med.* **2005**, *202*, 517–527. [CrossRef]
7. Xiao, H.; Wu, Z.; Li, B.; Shangguan, Y.; Stoltz, J.-F.; Magdalou, J.; Chen, L.; Wang, H. The low-expression programming of 11β-HSD2 mediates osteoporosis susceptibility induced by prenatal caffeine exposure in male offspring rats. *Br. J. Pharmacol.* **2020**, *177*, 4683–4700. [CrossRef]
8. Gregory, S.; Hill, D.; Grey, B.; Ketelbey, W.; Miller, T.; Muniz-Terrera, G.; Ritchie, C.W. 11β-hydroxysteroid dehydrogenase type 1 inhibitor use in human disease-a systematic review and narrative synthesis. *Metab. Clin. Exp.* **2020**, *108*, 154246. [CrossRef]
9. Chuanxin, Z.; Shengzheng, W.; Lei, D.; Duoli, X.; Jin, L.; Fuzeng, R.; Aiping, L.; Ge, Z. Progress in 11β-HSD1 inhibitors for the treatment of metabolic diseases: A comprehensive guide to their chemical structure diversity in drug development. *Eur. J. Med. Chem.* **2020**, *191*, 112134. [CrossRef]
10. Figaro-Drumond, F.V.; Pereira, S.C.; Menezes, I.C.; von Werne Baes, C.; Coeli-Lacchini, F.B.; Oliveira-Paula, G.H.; Cleare, A.J.; Young, A.H.; Tanus-Santos, J.E.; Juruena, M.F.; et al. Association of 11β-hydroxysteroid dehydrogenase type1 (HSD11b1) gene polymorphisms with outcome of antidepressant therapy and suicide attempts. *Behav. Brain Res.* **2020**, *381*, 112343. [CrossRef]
11. Krause, J.S.; Pérez, J.H.; Reid, A.M.A.; Cheah, J.; Bishop, V.; Wingfield, J.C.; Meddle, S.L. Acute restraint stress does not alter corticosteroid receptors or 11β-hydroxysteroid dehydrogenase gene expression at hypothalamic–pituitary-adrenal axis regulatory sites in captive male white-crowned sparrows (*Zonotrichia leucophrys gambelii*). *Gen. Comp. Endocrinol.* **2020**, *303*, 113701. [CrossRef] [PubMed]
12. Wan, Z.-K.; Chenail, E.; Li, H.-Q.; Ipek, M.; Xiang, J.; Suri, V.; Hahm, S.; Bard, J.; Svenson, K.; Xu, X.; et al. Discovery of HSD-621 as a potential agent for the treatment of type 2 diabetes. *ACS Med. Chem. Lett.* **2012**, *4*, 118–123. [CrossRef] [PubMed]
13. Shaabani, A.; Keshipour, S.; Shaabani, S.; Mahyari, M. Zinc chloride catalyzed three-component Ugi reaction: Synthesis of *N*-cyclohexyl-2-(2-hydroxyphenylamino)acetamide derivatives. *Tetrahedron Lett.* **2012**, *53*, 1641–1644. [CrossRef]
14. Kamiński, K.; Wiklik, B.; Obniska, J. Synthesis and anticonvulsant activity of new *N*-phenyl-2-(4-phenylpiperazin-1-yl)acetamide derivatives. *Med. Chem. Res.* **2015**, *24*, 3047–3061. [CrossRef]

15. Tang, Z.; Li, X.; Yao, Y.; Qi, Y.; Wang, M.; Dai, N.; Wen, Y.; Wan, Y.; Peng, L. Design, synthesis, fungicidal activity and molecular docking studies of novel 2-((2-hydroxyphenyl)methylamino)acetamide derivatives. *Bioorg. Med. Chem.* **2019**, *27*, 2572–2578. [CrossRef]

16. Shao, D.; Zhang, G.-N.; Niu, W.; Li, Z.; Zhu, M.; Wang, J.; Li, D.; Wang, Y. Design, Synthesis, and Cytotoxic Activity of 3-Aryl-*N*-hydroxy-2-(sulfonamido)propanamides in HepG2, HT-1080, KB, and MCF-7 Cells. *Chem. Biodivers.* **2019**, *16*, e1800646. [CrossRef]

17. Guo, J.; Chen, B.; Yu, Y.; Cheng, B.; Ju, Y.; Tang, J.; Cai, Z.; Gu, Q.; Xu, J.; Zhou, H. Structure-guided optimization and mechanistic study of a class of quinazolinone-threonine hybrids as antibacterial ThrRS inhibitors. *Eur. J. Med. Chem.* **2020**, *207*, 112848. [CrossRef]

18. Ibrahim, N.; Bonnet, P.; Brion, J.-D.; Peyrat, J.-F.; Bignon, J.; Levaique, H.; Josselin, B.; Robert, T.; Colas, P.; Bach, S.; et al. Identification of a new series of flavopiridol-like structures as kinase inhibitors with high cytotoxic potency. *Eur. J. Med. Chem.* **2020**, *199*, 112355. [CrossRef]

19. Zaręba, P.; Gryzło, B.; Malawska, K.; Sałat, K.; Höfner, G.C.; Nowaczyk, A.; Fijałkowski, Ł.; Rapacz, A.; Podkowa, A.; Furgała, A.; et al. Novel mouse GABA uptake inhibitors with enhanced inhibitory activity toward mGAT3/4 and their effect on pain threshold in mice. *Eur. J. Med. Chem.* **2020**, *188*, 111920. [CrossRef]

20. Wasfy, A.F.; Aly, A.A.; Behalo, M.S.; Mohamed, N.S. Synthesis of novel phthalazine derivatives as pharmacological activities. *J. Heterocycl. Chem.* **2020**, *57*, 12–25. [CrossRef]

21. Wang, M.-S.; Zhuo, L.-S.; Yang, F.-P.; Wang, W.-J.; Huang, W.; Yang, G.-F. Synthesis and biological evaluation of new MET inhibitors with 1,6-naphthyridinone scaffold. *Eur. J. Med. Chem.* **2020**, *185*, 111803. [CrossRef] [PubMed]

22. Oluwaseye, A.; Uzairu, A.; Shallangwa, G.A.; Abechi, S.E. Quantum chemical descriptors in the QSAR studies of compounds active in maxima electroshock seizure test. *J. King Saud Univ. Sci.* **2020**, *32*, 75–83. [CrossRef]

23. Praveenkumar, E.; Gurrapu, N.; Kolluri, P.K.; Yerragunta, Y.; Kunduru, B.R.; Subhashini, N.J.P. Synthesis, anti-diabetic evaluation and molecular docking studies of 4-(1-aryl-1H-1, 2, 3-triazol-4-yl)-1,4-dihydropyridine derivatives as novel 11-βhydroxysteroid dehydrogenase-1 (11β-HSD1) inhibitors. *Bioorg. Chem.* **2019**, *90*, 103056. [CrossRef]

24. Sharma, D.; Singh, A.; Pathak, M.; Kaur, L.; Kumar, V.; Roy, B.G.; Ojha, H. DNA binding and antiradical potential of ethyl pyruvate: Key to the DNA radioprotection. *Chem. Biol. Interact.* **2020**, *332*, 109313. [CrossRef] [PubMed]

25. Guo, Y.; Liu, X.; Zhang, Y.; Qiu, H.; Ouyang, F.; He, Y. 3-Bromopyruvate ameliorates pulmonary arterial hypertension by improving mitochondrial metabolism. *Life Sci.* **2020**, *256*, 118009. [CrossRef]

26. Szczuka, I.; Wiśniewski, J.; Kustrzeba-Wójcicka, I.; Terlecki, G. The effect of 3-bromopyruvate on the properties of cathepsin B in the aspect of metastatic potential of colon cancer cells. *Adv. Clin. Exp. Med. Off. Organ Wroc. Med. Univ.* **2020**, *29*, 949–957. [CrossRef]

27. Huang, Q.; Fu, Y.; Zhang, S.; Zhang, Y.; Chen, S.; Zhang, Z. Ethyl pyruvate inhibits glioblastoma cells migration and invasion through modulation of NF-κB and ERK-mediated EMT. *PeerJ* **2020**, *8*, e9559. [CrossRef]

28. Sun, X.; Sun, G.; Huang, Y.; Hao, Y.; Tang, X.; Zhang, N.; Zhao, L.; Zhong, R.; Peng, Y. 3-Bromopyruvate regulates the status of glycolysis and BCNU sensitivity in human hepatocellular carcinoma cells. *Biochem. Pharmacol.* **2020**, *177*, 113988. [CrossRef]

29. Kang, P.-W.; Su, J.-P.; Sun, L.-Y.; Gao, H.; Yang, K.-W. 3-Bromopyruvate as a potent covalently reversible inhibitor of New Delhi metallo-β-lactamase-1 (NDM-1). *Eur. J. Pharm. Sci.* **2020**, *142*, 105161. [CrossRef]

30. Gan, L.; Ren, Y.; Lu, J.; Ma, J.; Shen, X.; Zhuang, Z. Synergistic effect of 3-bromopyruvate in combination with rapamycin impacted neuroblastoma metabolism by inhibiting autophagy. *OncoTargets Ther.* **2020**, *13*, 11125–11137. [CrossRef]

31. Morris, G.M.; Huey, R.; Lindstrom, W.; Sanner, M.F.; Belew, R.K.; Goodsell, D.S.; Olson, A.J. Autodock4 and AutoDockTools4: Automated docking with selective receptor flexiblity. *J. Comput. Chem.* **2009**, *16*, 2785–2791. [CrossRef] [PubMed]

32. Frisch, M.J.; Trucks, G.; Schlegel, H.; Frisch, M.; Trucks, G.; Schlegel, H.; Scuseria, G.; Robb, M.; Cheeseman, J.; Scalmani, G.; et al. *Gaussian 09. Revision A.02*; Gaussian Inc.: Wallingford, CT, USA, 2009.

33. Zhang, J.; Osslund, T.D.; Plant, M.H.; Clogston, C.L.; Nybo, R.E.; Xiong, F.; Jordan, S.R. Crystal Structure of Murine 11β-Hydroxysteroid Dehydrogenase 1: An Important Therapeutic Target for Diabetes. *Biochemistry* **2005**, *44*, 6948–6957. [CrossRef] [PubMed]

34. Thomas, M.P.; Potter, B.V.L. Crystal structures of 11β-hydroxysteroid dehydrogenase type 1 and their use in drug discovery. *Future Med. Chem.* **2011**, *3*, 367–390. [CrossRef] [PubMed]

35. Yu, S.-J.; Zhu, C.; Bian, Q.; Cui, C.; Du, X.-J.; Li, Z.-M.; Zhao, W.-G. Novel ultrasound-promoted parallel synthesis of trifluoroatrolactamide library via a one-pot passerini/hydrolysis reaction sequence and their fungicidal activities. *ACS Comb. Sci.* **2014**, *16*, 17–23. [CrossRef]

36. Quiroga, D.; Becerra, L.D.; Sadat-Bernal, J.; Vargas, N.; Coy-Barrera, E. Synthesis and Antifungal Activity against Fusarium oxysporum of Some Brassinin Analogs Derived from l-tryptophan: A DFT/B3LYP Study on the Reaction Mechanism. *Molecules* **2016**, *21*, 1349. [CrossRef] [PubMed]